The Communication Distance of Non-Perennial Streams

Ken Aho[1], Dewayne Derryberry[2], Sarah E. Godsey[3], Rob Ramos[4], Sara Warix[3†], Sam Zipper[5]

[1]Department of Biological Sciences, Idaho State University, Pocatello, ID, USA, 83209-8007, [2]Department of Mathematics and Statistics, Idaho State University, Pocatello, ID, USA, 83209-8085, [3]Department of Geosciences, Idaho State University, Pocatello, ID, USA, [4]Division of Biology, Kansas State University, Manhattan, KS 66506, [5]Kansas Geological Survey, The University of Kansas, Lawrence, KS 66047-3724

Corresponding author: Ken Aho (kenaho@isu.edu)

[†]Current address: Hydrologic Science and Engineering, Colorado School of Mines, Golden, CO, USA.

Key Points:

- Conventional measures of stream connectivity are often poorly adapted to dynamic non-perennial stream networks that expand and contract.
- We developed Bayesian extensions to an existing stream length model, and a new Bayes-applicable metric called communication distance.
- Communication distance measures the capacity of a stream to bottleneck or allow material transfer from upstream to downstream locations.

This paper is a non-peer reviewed preprint submitted to EarthArXiv. The paper will be submitted for peer review to the journal *Water Resources Research*

Abstract

We developed Bayesian statistical approaches to assess non-perennial stream network connectivity. Our new methods allow: 1) consideration of changes to both local (stream segment) and global (stream network) connectivity over time, 2) incorporation of prior information from different data sources, and 3) straightforward computation of the posterior distributions of both active stream length and a new metric called communication distance. Communication distance measures the effective stream length for the movement of materials, including water and solutes, from upstream to downstream sites. Communication distance posteriors require the inverse-beta probability density function whose form had not been previously derived. The inverse-beta distribution can be used to represent the rarity of surface water presence compared to a perennial stream, thus clarifying bottlenecking propensities for stream segments. As an application, we considered Murphy Creek, a simple stream network in southwestern Idaho, USA. Our models used surface water presence/absence data from 2019, and priors based on existing regional USGS model predictions for surface water. Murphy Creek probabilities for surface water presence were heterogeneous in space and time, and were likely driven by fine-scale spatial variations in shallow subsurface hydraulic conductivity. Strong seasonal (spring, summer, fall) temporal differences were evident in network-level posterior distributions of both stream length and communication distance. Specifically, stream lengths were shorter and more variable in the summer and fall than in the spring. The novel communication distance posteriors were multimodal, platykurtic, and negatively skewed for spring, summer and fall, respectively, revealing bottlenecking effects that varied over time.

1 Introduction

Non-perennial streams comprise over half of the global river network (Messager *et al.,* 2021), are increasing in their spatial and temporal distribution (Zipper *et al*. 2021; Sauquet 2021), and strongly influence global water quantity and quality (Datry *et al*. 2014). Realization of the importance of non-perennial streams to large-scale hydrological, ecological, and biogeochemical processes has prompted increased study of these systems (Fovet *et al*., 2021). Nonetheless, characterization of non-perennial stream spatiotemporal dynamics remains challenging (Shanafield *et al.* 2021), inhibiting a clear understanding of linkages between stream drying and water quality.

Decreased stream connectivity from drying may affect water quality by preventing surface transport of materials. Numerous stream connectivity metrics exist (see reviews in Ali & Roy 2010, Bracken *et al*. 2013, Blume & Van Meerveld 2015) due in part to myriad perspectives concerning hydrologic connectivity (Ali & Roy 2009). These methods, however, have limitations for describing non-perennial streams. For example, several common measures of stream connectivity are time invariant due to their reliance on Cartesian grid relationships (e.g., Larsen *et al*. 2012, Trigg *et al*. 2013), or topography and drainage area (e.g., Jensco *et al*. 2009, Prancevic & Kirchner 2019). Thus, these measures may poorly describe non-perennial stream networks whose extent will vary in both time and space. Further, other stream connectivity measures, including those based on distances between “wet” locations (e.g., Western et al 2001, Ali and Roy 2010), or spatial autocorrelation structures (e.g., Knudby & Carrerra 2005, Ali & Roy 2010), provide only network-scale descriptions. Thus, these methods do not consider drying patterns at the scale of individual stream segments. This latter deficiency is particularly problematic in non-perennial streams because certain stream locations (e.g., surface flow bottlenecks) may have inordinately large effects on stream networks (Godsey and Kirchner 2014; Zipper *et al*. 2022a).

The variability of surface flow in non-perennial streams has driven the development and application of probabilistic models for surface water presence, often at watershed or larger spatial scales. These approaches include hidden Markov chain models based on stream temperature and conductivity (Arismendi *et al.* 2017), logistic models based on intermittency sensors and spatial data (Kaplan *et al*. 2020), and random forest classifications from remotely sensed geographic information system data (Sando and Blasch 2015, González-Ferreras and Barquín 2017, Jaeger *et al*. 2019). Recently, Botter & Durighetto (2020) developed a probability density function (PDF) approach to define distribution of stream network length, called the stream length duration curve (SLDC). A SLDC depicts the distribution of the "active" fraction of a stream network (i.e., the portion with surface flow), and provides the inverse of the exceedance probability of the total length of active streams for any outlet discharge. While these probabilistic approaches are commendable, they generally hold to a frequentist viewpoint which assumes a single "true" value for the probability of water presence at a stream segment. This view ignores diel and seasonal variation in the probability of stream segment water presence, and more importantly, prevents assessments of uncertainty and variability in probability designations.

Many sources of information concerning wetting and drying patterns may exist for a stream network, potentially based on multiple spatiotemporal scales and sampling schema. For example, it is possible that at a single watershed, stream surface flow has been: 1) modelled as part of subcontinent-scale research projects (e.g., USGS-PROSPER; Jaeger *et al*. 2019), 2) categorized into presence/absence outcomes at locations occasionally visited by local agencies or researchers, and 3) measured at a small number of locations using high-frequency intermittency sensors over days to years. Such prior information can be formally assimilated into Bayesian statistical analyses to inform and refine models based on current data (Gelman *et al.*, 2014). Weights can also be assigned to a prior based on data quality and the agreement of measurement scales of prior and current data. The resulting Bayesian posterior distribution allows straightforward assessments of variability and uncertainty in modelled phenomena. This approach seems particularly useful for depicting the probability of surface water presence in non-perennial streams, given the importance of quantifying central tendency and variation in this probability.

In this paper we develop Bayesian statistical methods to measure stream network connectivity that allow: 1) global (entire network) and local (stream segment) descriptions, 2) explicit consideration of the variability and uncertainty in probabilities of surface water presence, and 3) inclusion of prior information concerning probabilities of surface water presence. We also introduce a new metric called communication distance that quantifies the extent to which a stream segment or network blocks material transfer from upstream to downstream locations. Communication distance may improve understanding of the balance of transport, storage and reaction limitations within non-perennial networks and their downstream waters, whether they dry or not. Development of the communication distance metric prompted the first reported derivation of the inverse-beta distribution and its moments which we provide here.

2. Theoretical Foundation

2.1 Streams as graphs

For the sake of clarity and consistency, we consider non-perennial stream networks from the perspective of graph theory. A digraph (directed graph) is an ordered pair $D = (N, A)$, where N is a set of nodes and A is a set of arcs that link the nodes. If $a \in A$ is an arc with flow from node u to node v, we denote this as $a = \overrightarrow{uv}$, indicating that node u is the *tail* of arc a and v is the *head* of a. Aho *et al.* (2023) showed that directed acyclic graphs (DAGs) can be used to effectively depict stream networks. In a stream DAG, arcs can represent stream segments bounded by nodes at hydrologically meaningful locations such as sensor sites, confluences, splits, sources and sinks (Dodds and Rothman 2000, Rinaldo *et al*. 2006). A graph *cycle* occurs when a *path* starts and ends at the same node.

A digraph is *strongly connected* or *strong* if every node is reachable from every other node. A digraph is *weakly connected* if every node is reachable after replacing all oriented arcs with bidirectional arcs. In a *disconnected* digraph, nodes will remain isolated, even with bidirectional arcs. Thus, stream networks will be weakly connected under flowing conditions, and non-perennial streams will transition from weakly connected to disconnected digraphs as they dry (Fig 1).

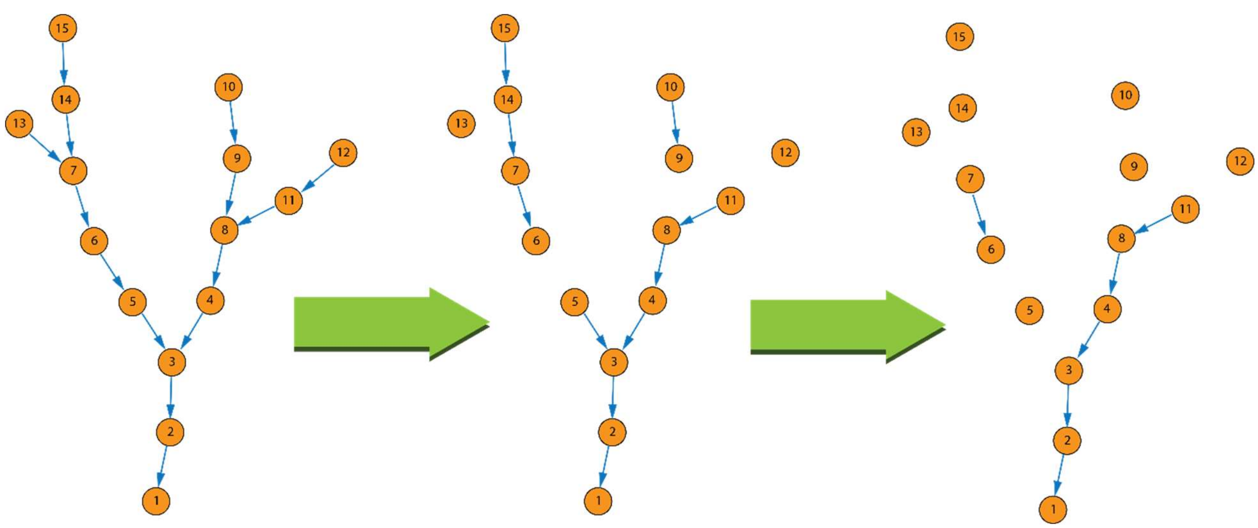

Figure 1. Conceptual DAG representation of a non-perennial stream through a representative drying event. From left to right, a fully wetted network with 15 nodes and 14 arcs (stream segments) dries to a network with only six arcs over time.

To increase the realism and usefulness of stream DAGs, weights can be overlain on arcs or nodes to represent physical stream properties including discharge, measured stream lengths, and/or probabilities of surface flow presence (Ort *et al*. 2009, Liu *et al*. 2022). The SLDC approach (Botter & Durighetto 2020) noted above, can be viewed as a weighted DAG representation of a stream network, with arcs weighted by the product of in-stream distance and the probability of surface water presence.

2.2 The Stream Length Duration Curve (SLDC) approach

In this section we briefly review the SLDC framework of Botter & Durighetto (2020), highlighting potential extensions and refinements. Let $\boldsymbol{X}$ = be a series of m Bernoulli random variables, $X_1, X_2, \dots, X_m$ representing surface water presence or absence at arcs (segments) in a stream network at the same point in time. Then, for the kth arc, $k = 1, 2, 3, \dots, m$, we have:

$$f(x_k) = p_k^{x_k}(1 - p_k)^{1-x_k} \quad (1)$$

where p_k is the probability that the kth arc is wet, and

$$x_k = \begin{cases} 1 & \text{if stream arc is wet} \\ 0 & \text{if stream arc is dry} \end{cases}.$$

Under its Bernoulli constraints, the mean and variance of X_k are

$$E(X_k) = p_k, \text{ and}$$

$$Var(X_k) = (1 - p_k)p_k.$$

Jointly, $\boldsymbol{X}$ is a multivariate Bernoulli random variable, with probability density function (Dai et al. 2013):

$$f(\boldsymbol{x}) = p_{0,0,\dots,0}^{\prod_{k=1}^{m}(1-x_k)} p_{1,0,\dots,0}^{x_1\prod_{k=2}^{m}(1-x_k)} p_{0,1,\dots,0}^{(1-x_1)x_2\prod_{k=3}^{m}(1-x_k)} \cdots p_{1,1,\dots,1}^{\prod_{k=1}^{m}x_k}. \quad (2)$$

where $p_{abc..z}$ is the joint probability of $X_1 = a, X_2 = b, X_3 = c, \dots, X_m = z$ and $\boldsymbol{x} = (x_1, x_2, \dots x_m)$ is a realization of $\boldsymbol{X}$.

Let Δl be an ordered vector of individual stream lengths for the set of fully wetted arcs: $\Delta l = \Delta l_1, \Delta l_2, \dots, \Delta l_m$, corresponding to binary surface water presence/absence outcomes in $\boldsymbol{X}$. Then, the dot product (sum of element-wise vector products), is a random variable, L, representing active stream network length:

$$L = \boldsymbol{X} \bullet \Delta l\,. \quad (3)$$

The resulting mean active stream network length is

$$E(L) = \sum_{k=1}^{m} p_k\, \Delta l_k,$$

(4)

and the active stream network length variance is

$$Var(L) = \sum_{i=1}^{m}\sum_{j=1}^{m} Cov(L_i, L_j).$$

(5)

where $Cov(L_i, L_j)$ denotes the covariance between stream lengths L_i and L_j. Note that for $k = i = j$, $Cov(L_k, L_k)$ is the kth arc variance, $Var(L_k) = \Delta l_k^2[p_k(1 - p_k)]$. This term will be the

kth diagonal entry in the variance covariance matrix for L, denoted $\boldsymbol{\Sigma_L}$. We refer to the approach defined in Eqs 1-5 as *Bernoulli stream length* due to its reliance on multivariate Bernoulli random variables. That is, Eq. 4 denotes the mean Bernoulli stream network length and Eq. 5 represents the variance of the Bernoulli stream network length.

Following Botter & Durighetto (2020), we recommend that all $p_k s$ be estimated using arithmetic means: $\hat{p}_k = n^{-1} \sum \boldsymbol{x}_k$, where $\boldsymbol{x}_k$ denotes binary surface water presence/absence data, taken over *n* trials, from the *k*th arc. Thus, we use $\boldsymbol{X}$ to represent a multivariate Bernoulli random variable signifying the presence/absence of surface water across the *m* arcs *in space*, i.e., $\boldsymbol{X} = (X_1, X_2, \dots X_m)$, $\boldsymbol{x}$ to represent a realization of $\boldsymbol{X}$ at one particular point in time $\boldsymbol{x} = (x_1, x_2, \dots x_m)$, and $\boldsymbol{x}_k$ to denote multiple Bernoulli outcomes from the *k*th arc *over time*: $\boldsymbol{x}_k = (x_{k,1}, x_{k,2}, \dots x_{k,n})$. This notation allows tracking of stream arc outcomes in both time and space. As noted above, for individual time events, $x_k \in \{0,1\}$.

Botter & Durighetto (2020) considered stream arc (segment) presence and stream arc lengths for upstream and downstream locations from a single node of interest. To allow extension of graph theory generalities, however, we recommend considering the presence/absence of surface water at arcs with respect to their bounding nodes. This approach clarifies delineation of the endpoints of stream arcs, and allows multiple estimation points for average arc surface water presence at a particular time. This approach prevents straightforward extension of node-based Bernoulli binary outcomes to arc presence/absence because the behavior of an arc's bounding nodes may not be identical. This issue, however, can be addressed using simulation approaches (see § 3.2 and Supplemental Materials S3).

Entries in $\boldsymbol{\Sigma_L}$ can be estimated with conventional method of moments-based variance and covariance estimators (see Aho 2014), using observed data, although pairwise correlations (standardized covariances) for arcs i and j should have the bounds (Botter & Durighetto, 2020):

$$\rho_{i,j}^{max} = \sqrt{\frac{p_j(1-p_i)}{p_i(1-p_j)}} \leq 1 \tag{6}$$

where $p_j \leq p_i$, and

$$\rho_{i,j}^{min} = \left(\frac{p_j p_i}{(1-p_i)i(1-p_j)}\right)^{\beta} \geq -1 \tag{7}$$

where $\beta = 1/2$ if $p_i + p_j \leq 1$ and $\beta = -1/2$ otherwise. Generalized covariance frameworks appropriate for stream networks can also be applied (see Cressie et al., 2006; Ver Hoef et al., 2006).

Botter and Durighetto (2020) present the distribution of L in terms of exceedance probabilities (one minus the cumulative distribution function of L). The inverse of this sigmoidal function represents the final form of the *SLDC*, in reflection of the widely-used flow duration curve (Castellarin 2004). Botter and Durighetto (2020) further consider stream hierarchical structures by ordering stream segments by their persistency and recognize the utility of hierarchical Bayesian perspectives in these efforts, but do not present components required for

Bayesian analyses, including likelihood functions, priors, and hyperparameter designations. Below we consider formal Bayesian approaches for modelling the probability of stream segment presence in non-perennial streams.

2.3 Modeling the probability of surface water – Bayesian extensions to the SLDC

Several approaches can be used to represent the probability of surface water presence at the kth arc (segment) as a random variable, θ_k. One possibility is to define θ_k as a beta random variable with a mean equivalent to an estimated probability of surface water presence, $\hat{p}_k$. Under this approach, the distribution of θ_k can be defined using only the first beta distribution shape parameter, α. Specifically, let

$$\theta_k \sim BETA(\alpha, \beta = r\alpha) \quad (8)$$

for some $\alpha > 0$, where $\frac{1}{1+r}$ is equal to the estimated probability of surface water presence, $\hat{p}_k$, and, as a result $r = \frac{1-\hat{p}_k}{\hat{p}_k}$. Then,

$$\begin{aligned} E(\theta_k) &= \frac{\alpha}{\alpha + \beta} \\ &= \frac{\alpha}{\alpha + r\alpha} \\ &= \frac{1}{1 + r} = \hat{p}_k. \end{aligned}$$

This approach can be applied within the Bayesian framework:

$$f(\theta_k|\boldsymbol{x}_k) \propto f(\boldsymbol{x}_k|\theta_k) f(\theta_k) \quad (9)$$

where $f(\theta_k|\boldsymbol{x}_k)$ is the posterior density function for the probability of surface water at the kth stream segment, given *n* observed binary presence/absence outcomes from the kth segment. As before, $\boldsymbol{x}_k = (x_{k,1}, x_{k,2}, \ldots x_{k,n})$. In this application, $f(\boldsymbol{x}_k|\theta_k)$ would conventionally be represented as a binomial likelihood function, describing the likelihood of surface water presence from the kth stream segment over time, given probabilities of surface water presence, θ_k. That is, $\boldsymbol{x}_k|\theta_k \sim BIN(n, \theta_k)$. Given this likelihood family, it is expedient to employ conjugate beta prior distributions, $\theta_k \sim BETA(\alpha, \beta)$, resulting in posteriors that are also beta distributed. Conjugacy is useful in Bayesian analyses because the posterior distribution will have a known parametric form (Gelman et al. 2014, pg. 34), allowing straightforward summarization of the posterior, and diminishing the need for complex numerical procedures, including Markov Chain Monte Carlo (MCMC) approaches.

Conventional naïve beta priors include $BETA(1,1)$, $BETA(0.5,0.5)$, i.e., the Jeffreys prior, and $BETA$ (0, 0). All three priors attribute equal degrees of belief to wet and dry stream outcomes. In fact, the $BETA(1,1)$ prior will give equal densities (of one) to all possible probabilities of surface water presence in the interval $(0,1)$. The three distributions, however connote decreasing effective prior sample sizes, and thus decreasing overall weights for the prior compared to the current data. The prior distribution with the smallest effective sample size, $BETA(0, 0)$, results in a posterior whose mean will equal the arithmetic mean of the current data, although in this case a proper posterior (one with a finite integral) requires that at least one water presence and one water absence outcome are actually observed.

Informative beta priors can also be used depending on the availability and quality of prior information that is extraneous to *current data* used in the likelihood. As noted above, informative beta priors for θ_k can be defined in which $E(\theta_k)$ is a prior estimate of the probability of surface water presence at the *k*th arc (Eq. 8). Our particular application of this approach is described in Section 3.2.1.

Given beta priors and binomial likelihoods, the posterior density function will have the form $\theta_k|\boldsymbol{x}_k \sim BETA(\alpha + \sum \boldsymbol{x}_k, \beta + n - \sum \boldsymbol{x}_k)$ where α and β are values defined for the beta distribution shape hyperparameters in the prior. Under linear transformation, the posterior distribution for the length of the kth arc can be obtained by multiplying the $\theta_k|\boldsymbol{x}_k$ posterior by the constant Δl_k. A Bayesian depiction of the average stream length for the entire network can be obtained by taking the sum of the product $E(\theta_k|\boldsymbol{x}_k) \cdot \Delta l_k$, across all segments This general approach is also well suited for communication distance, discussed next.

2.4 Communication distance

The concept of stream length may be non-informative or even misleading with respect to the internodal communication and transport of materials. For example, for spatially adjacent nodes u and v, the drying of the connecting stream arc means that the distance from u to v with respect to surface transport of flow-borne organisms and resources has become infinite, although the Bernoulli stream length for the arc is zero. To measure resource transport constraints within stream networks we propose a new metric, *communication distance*, denoted C. Following Botter & Durighetto (2020) we represent stream arc lengths using $\Delta l_k \in \{\Delta l_1, \Delta l_2, \dots, \Delta l_m\}$, and corresponding probabilities for surface water presence as $p_k \in \{p_1, p_2, \dots, p_m\}$. Then the communication distance of the *k*th arc is:

$$C_k = \frac{\Delta l_k}{p_k}$$

and the network communication distance is:

$$C = \sum_{k=1}^{m} C_k . \tag{10}$$

Given all $p_k = 1$, the network communication distance will equal network the Bernoulli stream length, which in this case will be $\sum_{k=1}^{m} \Delta\, l_k$. Given any $p_k = 0$, the network communication distance becomes ∞. Clearly, however, for any arc k to be correctly defined as a stream segment, $\forall p_k > 0$ over an extended time span, making $C < \infty$. For $0 < p_k \leq 1$, the network communication distance will be $\sum_{k=1}^{m} \Delta\, l_k \leq C < \infty$.

As noted earlier, when considering random variability in p_k, the posterior distribution of $E(L_k)$ can be obtained as the product of the *k*th beta posterior for the probability of surface water presence and the *k*th stream length. Acquisition of the posterior distribution of $E(C_k)$ is less straightforward, however, because this requires multiplication of the *k*th stream length by the multiplicative inverse of the *k*th beta posterior.

If Y_k follows a beta distribution then Y_k^{-1} will follow an inverse-beta distribution. Prior to our efforts this distribution had not been derived, although as a practical matter it is straightforward to obtain inverse-beta outcomes from existing computer algorithms (e.g., `1/rbeta()` in the **R** computational environment). Mathematical derivations of the inverse-beta distribution and its moments are given in the Supplementary Materials, Appendix S1.

If $Y_k \sim BETA(\alpha, \beta)$, with $\alpha, \beta > 0$, then $Y_k^{-1} \sim BETA^{-1}(\alpha, \beta)$ with PDF:

$$f(y_k^{-1}) = \frac{\Gamma(\alpha+\beta)}{\Gamma(\alpha)\Gamma(\beta)} \left(\frac{1}{y_k^{-1}}\right)^{\alpha+1} \left(1 - \frac{1}{y_k^{-1}}\right)^{\beta-1}, \tag{11}$$

mean,

$$E(Y_k^{-1}) = \frac{\alpha+\beta-1}{\alpha-1}, \tag{12}$$

and variance

$$Var(Y_k^{-1}) = \frac{(\alpha+\beta-1)}{\alpha-1} \cdot \frac{\beta}{(\alpha-1)(\alpha-2)}. \tag{13}$$

As suggested above, the inverse beta distribution can be used to represent distributions of reciprocal probabilities which will occur in (1, ∞], given probabilities in (1,0]. Reciprocal probabilities are useful for measuring the rarity of outcomes. Specifically, the reciprocal probability, *r*, for an outcome *A*, indicates that there is a 1 in *r* chance that *A* will occur. For instance, if the probability of surface water presence is 0.01, then one would expect that surface water will occur in 1 of 100 cases, because *r* = 1/0.01 = 100.

Let $(\theta_k|\boldsymbol{x}_k)^{-1}$ be an inverse beta posterior distribution of the reciprocal probability of surface water presence at the *k*th arc, then the posterior mean communication distance for the kth arc is:

$$E(C_k) = \Delta l_k E[(\theta_k|\boldsymbol{x}_k)^{-1}], \tag{14}$$

and the posterior average network communication distance is:

$$E(C) = \sum_{k=1}^{m} \Delta\, l_k E[(\theta_k|\boldsymbol{x}_k)^{-1}]. \tag{15}$$

The posterior communication distance variance of the kth arc is:

$$Var(C) = \Delta l_k^2 Var[(\theta_k|\boldsymbol{x}_k)^{-1}], \tag{16}$$

and the posterior communication distance variance of the entire network is:

$$Var(C) = \sum_{i=1}^{m}\sum_{j=1}^{m} Cov(C_i, C_j) \tag{17}$$

where $Cov(C_i, C_j)$ denotes the covariance between communication distances C_i and C_j. For $k = i = j$, $Cov(C_k, C_k)$ is the kth marginal variance, $Var(C_k)$.

3 Materials and Methods

3.1 Field site and field methods

We derived Bernoulli stream length and communication distance summaries for Murphy Creek, a simple drainage system within the larger Reynolds Creek experimental watershed in the Owyhee Mountains of southwestern Idaho, USA (Fig. 2; Warix et al., 2021). Measures of stream surface presence were made at 25 nodes, corresponding to 24 stream arcs. We designated additional (un-instrumented) graph nodes at the outlet and at two stream sources, resulting in a total of 27 nodes and 26 arcs. At 21 nodes, surface water presence was measured with sensors (Onset HOBO Pendant/Light 64 K Datalogger sensors (UA002-64) that were modified to detect resistivity (Chapin et al., 2014). The resistivity sensors were located in the deepest part of the channel and installed so that the two pole electrodes were touching the stream bed and thus able to detect the presence or absence of water at the lowest of flow conditions. At four other sites, stream specific conductivity was used to detect water levels for baseflow monitoring, allowing detection of the absence of stream surface water presence (Fig. 2). These measures were obtained with HOBO pressure transducers (Onset Hobologger, U-24). Surface water presence/absence was determined every 15 minutes from 6/3/2019 to 10/2/2019. Additional details can be found in Warix et al. (2021).

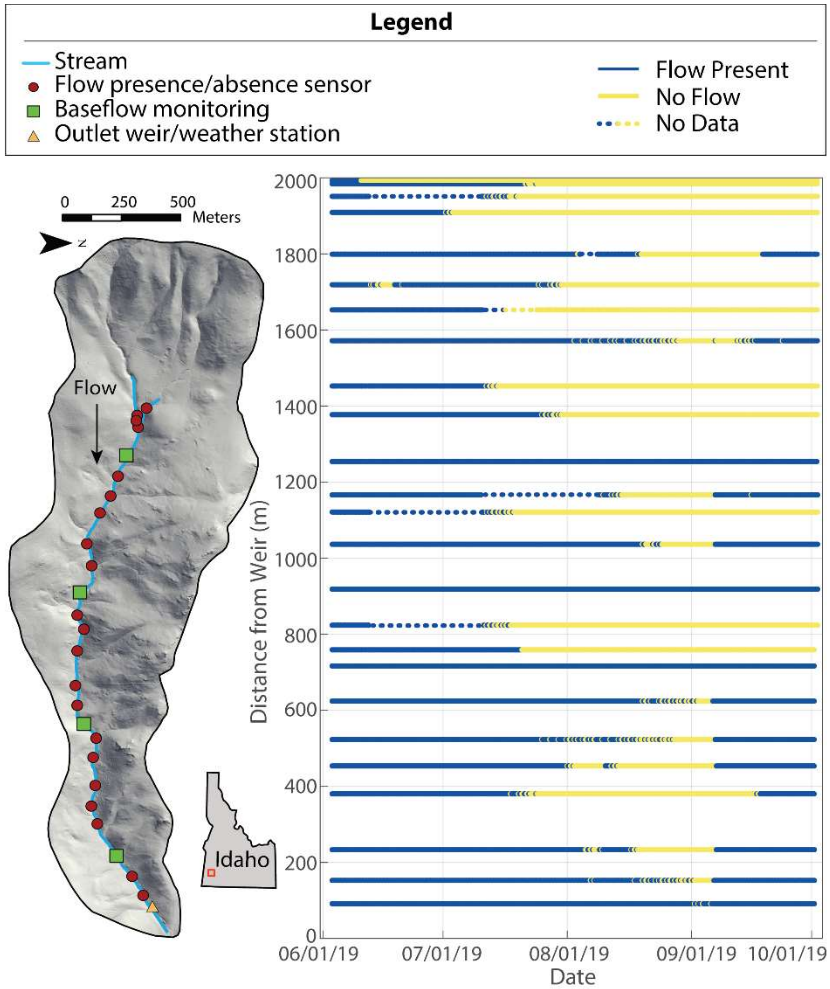

Figure 1. Instrumentation of the Murphy Creek sub-watershed in 2019 (outlet coordinates: 43.25607°, -116.8186°) and summary of flow presence over the seasonal recession at each sensor.

3.2 Statistical methods

We created inferential models of Bernoulli stream length and network communication distance at Murphy Creek based on the entirety of the sampling period, and on three seasonal subsets: spring (6/3/2019 - 7/10/2019), summer (7/11/2019 - 9/14/2019), and fall (9/15/2019 - 10/2/2019). Seasonal cutoffs were established subjectively at dates representing approximate change points in precipitation and temperature, following examination of long-term (1964-1996) climate trends for the study area (Hanson *et al.* 2001) for days of the year corresponding to the 2019 sampling period (early June to Early October). Probabilities of the presence of surface water at arcs were calculated, based on the dry/wet conditions of their bounding nodes over the entire sampling period or during periods representing spring, summer and fall. Specifically, for the kth arc with bounding nodes u and v, for the ith time frame, $i = 1,2,3, \dots, n$, we applied the following rule to obtain arc outcomes from our nodal sensor datasets:

$$x_{k,i} = \begin{cases} 1.0, & \text{both } u \text{ and } v \text{ wet} \\ 0.0, & \text{both } u \text{ and } v \text{ dry} \\ 0.5, & \text{only one of } u \text{ or } v \text{ wet} \end{cases}. \tag{18}$$

Marginal (individual arc) probabilities of surface water presence and covariances among arcs were both estimated using these derived arc outcomes. Exceptions were the three arcs associated with input and sink locations, whose extremal nodes were not instrumented (Fig. 2). In this case, surface water outcomes were based on water presence/absence outcomes at the nearest measured node.

We used the **R** package *mipfp* (Barthélemy & Suesse, 2018) to generate multivariate Bernoulli trials for water presence at arcs based on estimated arc marginal probabilities of water presence and inter-arc covariances. Specifically, we generated 1000 random multivariate Bernoulli trials, each made up of $m = 26$ potentially correlated binary outcomes, representing the simultaneous presence or absence of surface stream flow at each of the 26 designated Murphy Creek stream arcs. We applied this step using estimates from data for the entire sampling period, and for separate data subsets representing spring, summer, and fall. We used this simulation approach to address the issue of potential non-binary outcomes resulting from Eq. 18, and the fact that surface water presence at arcs is often positively correlated in both space and time. Our approach allowed generation of large arc surface water presence or absence datasets made up of temporally independent (random) samples representative of *particular spans of time*, i.e., the entire sampling period, spring, summer, and fall, based on the estimated marginal probabilities for stream segment presence and the estimated spatial dependencies of arcs during those periods of time. We randomly sampled with replacement with a sample size of $n = 10$ from the collections of random multivariate Bernoulli outcomes 10000 times, for the entire sampling period, and for each season, and used the numbers of successes (i.e., surface water presence outcomes) from those ten trial simulations as multivariate binomial outcomes in subsequent analyses. We note that the sample size used was largely irrelevant from the perspective of Bayesian inference. This is because we defined the prior effective sample size to be a fixed proportion of the data sample size, for any n (see § 3.2.1 below, and additional considerations in § 5.4).

3.2.1 Bayesian methodology

Under our Bayesian framework, simulated binomial data outcomes obtained from *mipfp* algorithms were coupled with beta priors to obtain beta posteriors. Informative beta priors were defined (see Eq 8) to have a mean corresponding to the 2004-2016 average from the Probability of Streamflow Permanence model (PROSPER; Jaeger et al. 2019), as reported for Murphy Creek stream segments by the United States Geological Survey (USGS) StreamStats web-based application (USGS, 2016). The PROSPER model uses a random forest classifier to estimate the probability of surface water for a large number of stream networks and associated stream segments in the Pacific Northwest, USA (Jaeger et al. 2019).

The effective sample size for a beta prior is the sum of its hyperparameters, α and β, whereas the effective sample size for the data is n (Morita et al., 2008). We defined the prior hyperparameters so that effective sample size for the prior was a fixed proportion, w, of n. That is, we let: $\alpha + \beta = w \cdot n$. Because the parameterization for our priors was $\theta_k \sim BETA(\alpha, \alpha r)$, where $r = \frac{1-\hat{p}_{k(prosper)}}{\hat{p}_{k(prosper)}}$, this required that $\alpha + \alpha \cdot r = w \cdot n$, resulting in:

$$\alpha = w \cdot n \cdot \hat{p}_{k(prosper)}, \text{ and}$$
$$\beta = w \cdot n\left(1 - \hat{p}_{k(prosper)}\right).$$

Under this framework, the posterior distribution for the probability of surface water presence at the *k*th arc had the form:

$$\theta_k | \boldsymbol{x}_k \sim BETA\left(w \cdot n \cdot \hat{p}_{k(prosper)} + \sum \boldsymbol{x}_k, w \cdot n\left(1 - \hat{p}_{k(prosper)}\right) + n - \sum \boldsymbol{x}_k\right), \quad (19)$$

with mean

$$E(\theta_k | \boldsymbol{x}_k) = \frac{w \cdot n \cdot \hat{p}_{k(prosper)} + \sum \boldsymbol{x}_k}{w \cdot n \cdot \hat{p}_{k(prosper)} + w \cdot n\left(1 - \hat{p}_{k(prosper)}\right) + n}, \quad (20)$$

and variance:

$$Var(\theta_k | \boldsymbol{x}_k) = \frac{w \cdot n \cdot \hat{p}_{k(prosper)} + \sum \boldsymbol{x}_k}{\left[w \cdot n \cdot \hat{p}_{k(prosper)} + w \cdot n\left(1 - \hat{p}_{k(prosper)}\right) + n\right]^2} \cdot \frac{w \cdot n \cdot \left(1 - \hat{p}_{k(prosper)}\right) + n - \sum \boldsymbol{x}_k}{w \cdot n \cdot \hat{p}_{k(prosper)} + w \cdot n\left(1 - \hat{p}_{k(prosper)}\right) + n + 1} \quad (21)$$

The sum of the products of the beta posterior means and respective segment lengths across all *m* arcs, $\sum_{k=1}^{m} E(\theta_k | \boldsymbol{x}_k) \cdot \Delta l_k$, defined a posterior distribution outcome for mean Bernoulli stream length, $E(L)$.

The inverse-beta posterior distribution for reciprocal probability of surface water presence at the *k*th arc (required for derivation of the *k*th arc communication distance posterior) was:

$$(\theta_k | \boldsymbol{x}_k)^{-1} \sim BETA^{-1}\left(w \cdot n \cdot \hat{p}_{k(prosper)} + \sum \boldsymbol{x}_k, w \cdot n\left(1 - \hat{p}_{k(prosper)}\right) + n - \sum \boldsymbol{x}_k\right). \quad (22)$$

Thus, the mean of the *k*th inverse-beta posterior was:

$$E[(\theta_k|\boldsymbol{x}_k)^{-1}] = \frac{w \cdot n \cdot \hat{p}_{k(prosper)} + \sum \boldsymbol{x}_k + w \cdot n\left(1 - \hat{p}_{k(prosper)}\right) + n - \sum \boldsymbol{x}_k - 1}{w \cdot n \cdot \hat{p}_{k(prosper)} + \sum \boldsymbol{x}_k - 1} \tag{23}$$

and the variance of the *k*th inverse-beta posterior was:

$$Var[(\theta_k|\boldsymbol{x}_k)^{-1}] = \frac{w \cdot n \cdot \hat{p}_{k(prosper)} + \sum \boldsymbol{x}_k + w \cdot n \cdot \left(1 - \hat{p}_{k(prosper)}\right) + n - \sum \boldsymbol{x}_k - \mathbf{1}}{w \cdot n \cdot \hat{p}_{k(prosper)} + \sum \boldsymbol{x}_k - 1} \cdot \frac{w \cdot n \cdot \left(1 - \hat{p}_{k(prosper)}\right) + n - \sum \boldsymbol{x}_k}{\left[w \cdot n \cdot \hat{p}_{k(prosper)} + \sum \boldsymbol{x}_k - 1\right]\left[w \cdot n \cdot \hat{p}_{k(prosper)} + \sum \boldsymbol{x}_k - 2\right]} \tag{24}$$

The sum of the products of the inverse-beta posterior means and respective segment lengths, $\sum_{k=1}^{m} E[(\theta_k|\boldsymbol{x})^{-1}] \cdot \Delta l_k$, was used to define a posterior outcome for $E(C)$.

We weighted the beta priors so that they would have 50% of the weight of the sample data and, as noted above, let the sample size be 10 random draws from a multivariate Bernoulli distribution simulated from 2019 field data. That is, for equations 18-24 above, we let $w = 0.5$, $n = 10$, and, thus $\sum \boldsymbol{x}_k \in \{0,1,2,\ldots,10\}$.

3.3 Software

The **R** statistical environment (R Core Team 2022) was used for all analyses with reliance on the package *streamDAG* (Aho 2022), which allowed straightforward computation of Bernoulli stream length and communication distance posteriors, and the package *mipfp* (Barthélemy & Suesse, 2018) for simulation of multivariate Bernoulli outcomes. Several spatial and graphics packages, including *sf* (Pebesma 2018), *ggspatial* (Dunnington 2021), *cowplot* (Wilke 2020), *ggplot2* (Wickham 2016), and *gridGraphics* (Murrell and Nen 2020) were also used to visualize the results.

4 Results

4.1 Comparisons of prior, observed, and posterior probabilities of surface water presence

The probabilities of surface water presence diverged for the prior and the 2019 field data for some stream segments. Specifically, PROSPER prior probabilities for surface water presence were limited to the range 0.21-0.32 (Fig 3a), whereas field observations in 2019 included reaches that were (nearly) always wet or dry (Fig 3b). By definition, posterior probabilities (Fig 3c) were a compromise between the PROSPER priors and 2019 observations (also see Aho 2014, pgs. 137-142).

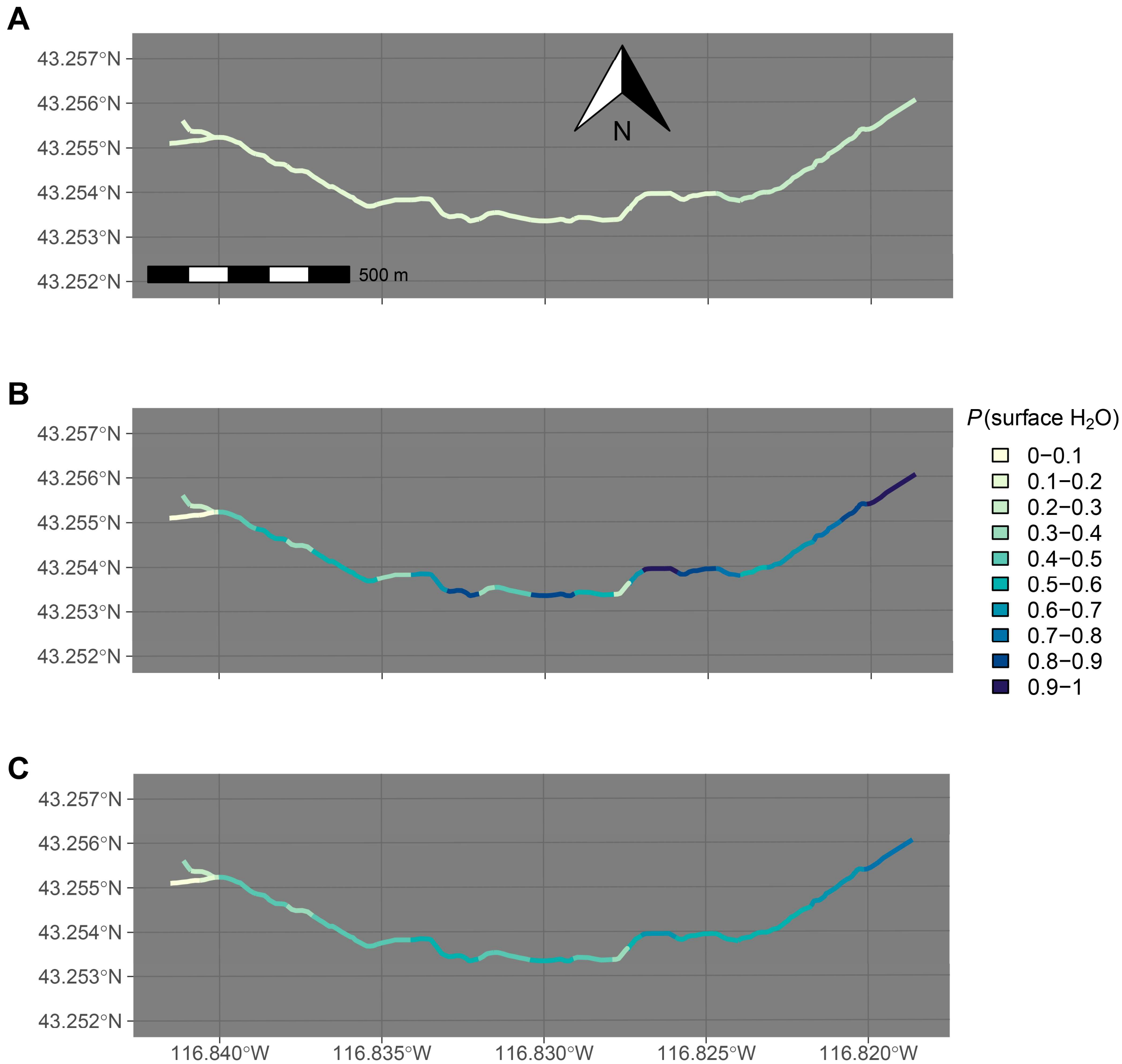

Figure 3. Spatially distributed probabilities of stream surface water presence at Murphy Creek with flow proceeding from left to right (see Fig. 2). Panel (a) depicts surface water presence probabilities from the USGS-PROSPER model, which were used as means for beta distribution priors in Bayesian analyses. Panel (b) shows probabilities based solely on surface water presence/aabsence data from the entire 2019 sampling period, from 06/03/2019 to 10/03/2019. Panel (c) depicts means from beta posterior distributions representing the probability of stream surface water presence.

4.2 Quantifying uncertainty in reach-scale wet/dry predictions: Posterior distributions for the probability of surface water for individual arcs

Our approach summarized both intra-arc central tendency and the variability in the probability of surface water presence (Fig 4). Consistent with arc prior distributions (Fig 3a), posterior beta distributions of arcs nearer the outlet generally had larger mean values (Fig 3c), indicating high average probabilities of surface water presence (Fig 4b). Arcs near the top and bottom of the network had low variability in the probability of surface water. Posterior distributions for arcs near the outlet, e.g., $\overrightarrow{M91\ OUT}$, had smaller variances because surface water was generally present at these locations, whereas arc posteriors near inputs, e.g., $\overrightarrow{INS\ M1993}$, had smaller variances because surface water was generally absent (Fig 4b). Critically, arc distributions near the middle of the stream had platykurtic posteriors with relatively large variances.

4.3 Identifying bottleneck locations: Posterior distributions for the reciprocal probability of surface water presence for individual arcs

The symmetry and kurtosis of arc of inverse-beta posteriors (Fig 5) varied much more strongly than arc distributions for the (non-reciprocal) probability of surface water presence (Fig 4). Arc distributions near the top of the network were strongly platykurtic with relatively large means, indicating that, on average, surface water was rare, whereas arc distributions near the outlet were leptokurtic, with much of the probability mass near one, indicating the arc resembled a perennial stream segment. A large inverse-beta mean at $\overrightarrow{M823\ M759}$ indicated a strong potential for a mid-stream communication bottleneck (Fig 5b).

4.4 Assessing network-scale effects: Comparison of stream length, L, and communication distance, C

Distributions of average stream length and communication distance varied dramatically in the spring, summer and fall (Fig 6). Greater distinctions were evident for the distributions of $E(C)$ compared to $E(L)$. Specifically, while the posterior distributions of $E(L)$ were symmetric across seasons (Fig 6b), posterior distributions of $E(C)$ were highly complex and asymmetric (Fig 6c). For example, the spring posterior distribution of $E(C)$ was multimodal, while the summer and fall posteriors for $E(C)$ were strongly platykurtic and negatively skewed, respectively (Fig 6c).

A fall rewet period was evident for Bernoulli stream lengths, with fall average streams being longer than those of summer (Fig 6a,b). This trend was not evident for the communication distance posterior distribution, as larger communication distances occurred in the fall compared to the summer (Fig 6c). The probability distribution of $E(C)$ in the fall appeared highly compact (Fig 6b) because of the conflation of its large magnitude outcomes and the requirement that the area under a valid PDF be one.

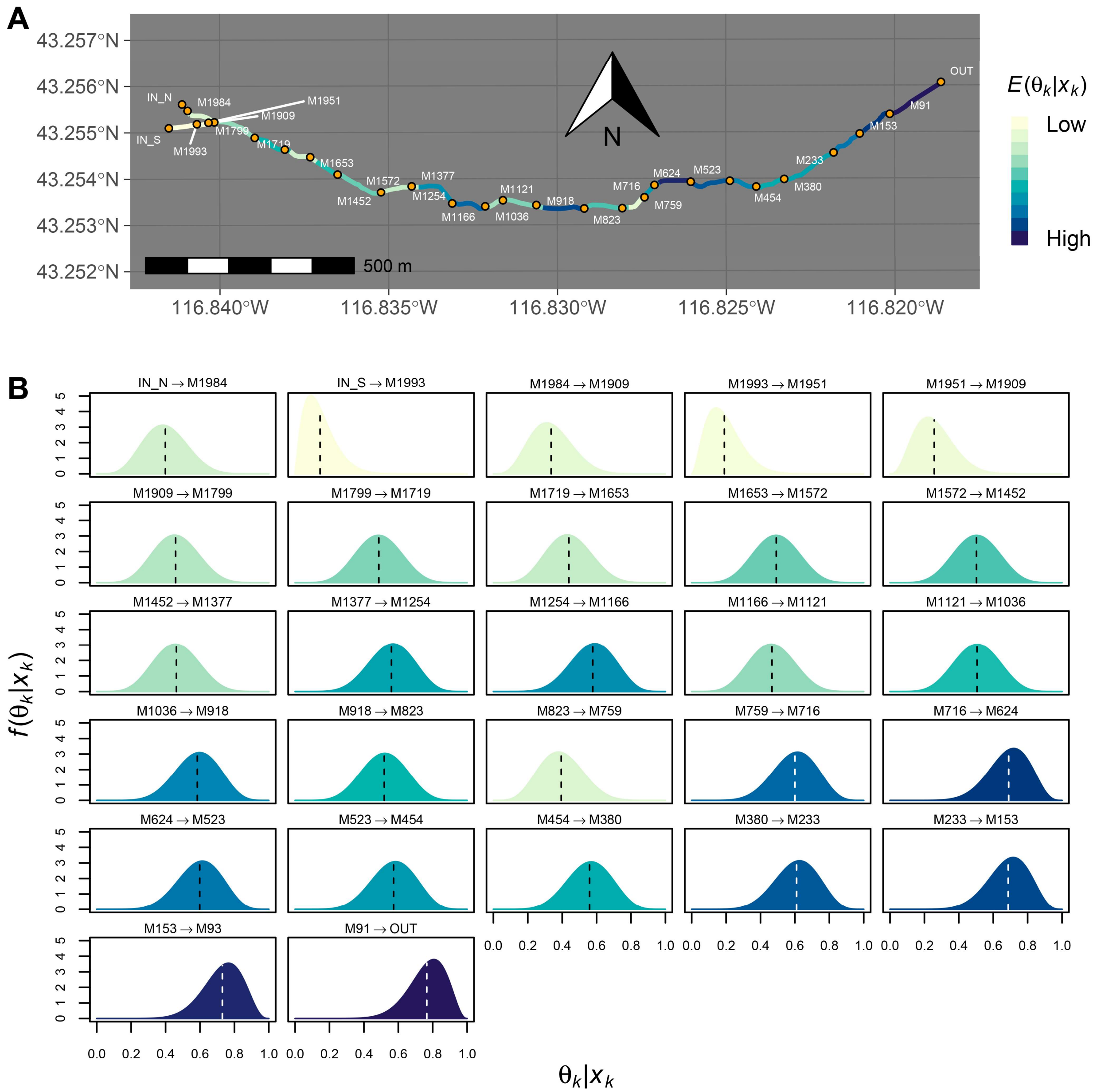

Figure 4. Summaries of posterior beta distributions for Murphy Creek stream segments from 06/03/2019 to 10/02/2019, representing the probability of surface water presence. Names of arc bounding nodes correspond to meter distances upstream from the outlet. Panel (a) locates nodes along the network. Arcs are colored by their posterior distribution mean values (see key). Larger means (darker, bluer colors) indicate arcs with a higher propensity for surface water presence outcomes. Panel (b) shows beta posterior distributions for each arc. Arc posterior distributions are sorted, by row, from sources to outlet. Arc posterior distributions are colored based on their mean values, and follow the same color ramp as (a). Posterior means for arcs are overlain with dashed lines.

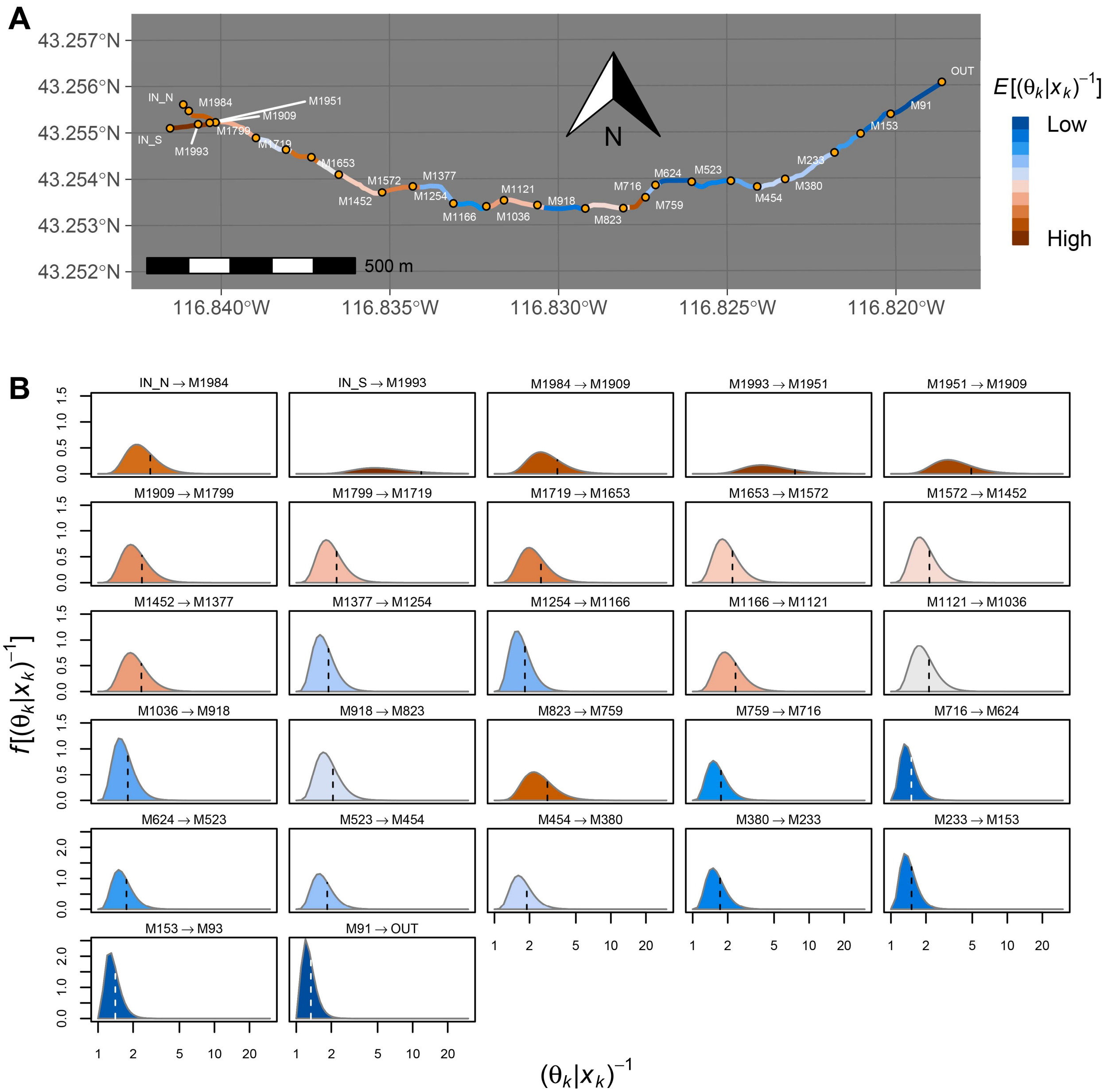

Figure 5. Summaries of posterior inverse-beta distributions for Murphy Creek arcs from 06/03/2019 to 10/02/2019, representing the reciprocal probability of surface water presence. Thus, increasing values indicate increased *rarity* of surface water at an arc, or increased likelihood that arc might act as a bottleneck for material transport. Names of arc nodes correspond to meter distances upstream from the outlet. Panel (a) locates nodes along the stream network. Arcs are colored by their posterior distribution mean values (see key). Larger means (redder colors) indicate arcs for which surface water presence is increasingly rare. Panel (b) shows inverse-beta posterior distributions for each arc. Arc distributions are sorted, by row, from sources to outlet. Arc posterior distributions are colored based on their mean values, following the color ramp from (a). Posterior means are overlain on the distributions with dashed lines. Note that *y*-axis limits differ for the last two rows of PDFs in (b) because of their leptokurtic shapes.

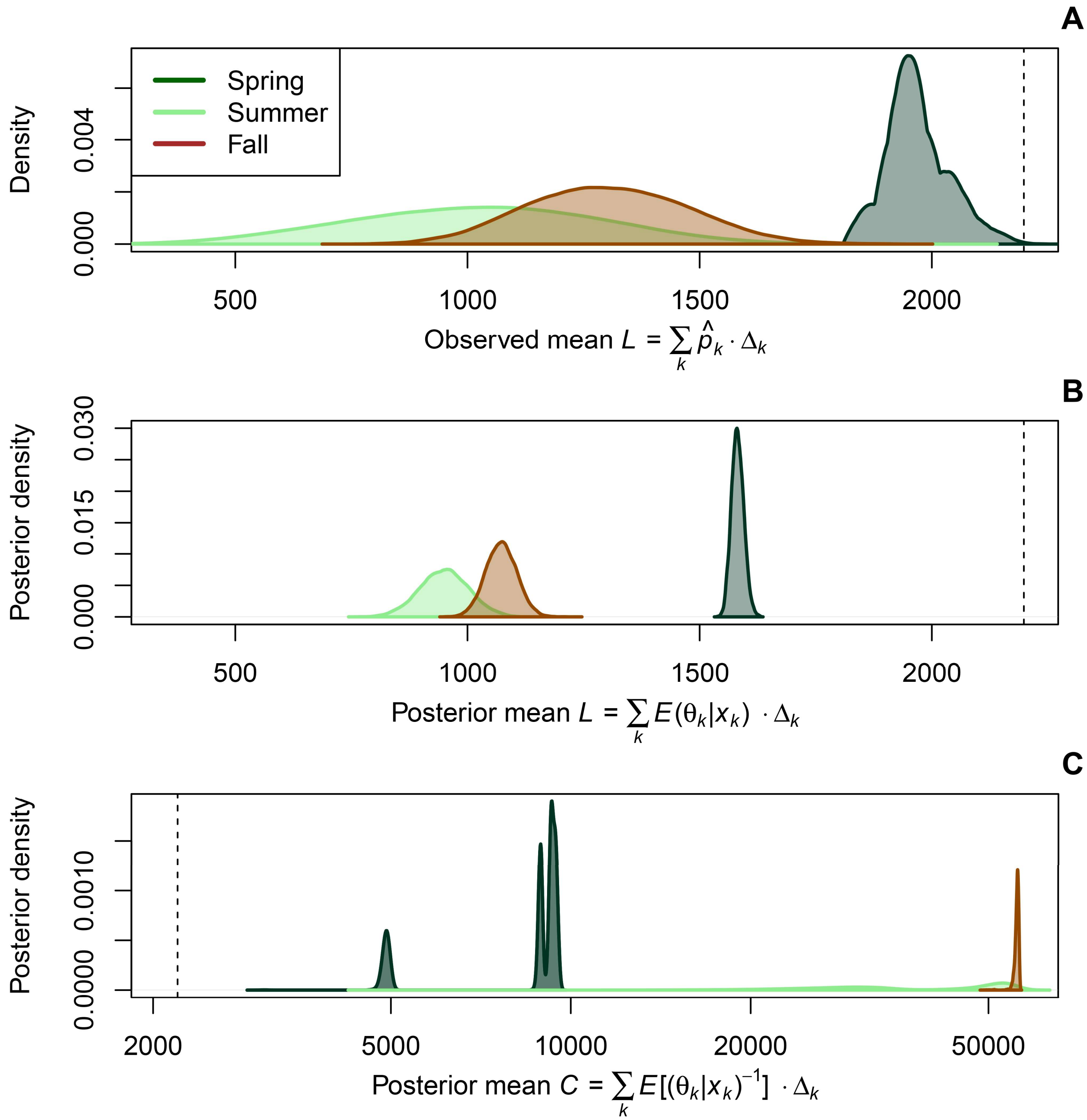

Figure 6. Seasonal distributions of stream length and communication distance. Panel (a) shows observed mean stream length (in meters) based on random outcomes from a multivariate Bernoulli distribution with parameters based on 2019 data (see Section 3.2). Panel (b) shows Bernoulli posterior mean stream length (in meters) for the network. Panel (c) shows posterior mean communication distance for the network. Note the log scale of the *x*-axis in panel (c). Expressions of density in plots are based on a Gaussian smoothing kernel. The fully-wetted stream length of Murphy Cr. is denoted with a vertical dashed line in (a-c).

5 Discussion

We developed Bayesian measures of non-perennial streams connectivity that: 1) allowed global (network-scale) and local (stream segment or reach-scale) perspectives on hydrological connectivity, 2) quantified variability in intra-segment surface flow presence probabilities, and 3) allowed the inclusion of prior information concerning probabilities of surface flow presence. Our novel contributions include Bayesian extensions of Bernoulli stream network length (Botter & Durighetto 2020) and communication distance, a novel metric that quantifies the effective stream length for material transfer from upstream to downstream locations. Our approaches allow probabilistic consideration of questions of particular relevance to stream researchers. For instance: "What is the probability that the effective network length will be longer during the spring compared to summer?" Or: "What is the probability that the effective stream length for communication of materials of a non-perennial segment will become more than q times as large as a comparable perennial segment?" Bayesian application of communication distance prompted derivation of the inverse-beta probability density function which can be used to represent a distribution of reciprocal probabilities of surface water presence. We tested our new approaches by determining Bayesian posterior distributions of the probability and reciprocal probability of surface water presence for individual stream arcs (segments) at Murphy Creek, a simple non-perennial stream network in southwestern Idaho, USA. Results for Murphy Creek stream arcs were used to generate network-level posterior distributions of Bernoulli stream length and communication distance across three seasons.

5.1 Predicting drying patterns from fine-scale observations

Stream drying at Murphy Creek was heterogeneous in space over time (Figs 3-5), consistent with the varying importance of groundwater contributions to patterns of flow probability (Warix *et al*., 2021). Sustaining surface flow via groundwater requires that groundwater is both present in the shallow subsurface and that shallow subsurface properties allow water to flow from the subsurface into the stream or preclude its rapid loss (e.g., Dohman *et al*. 2021). Figure 7 shows two proximal Murphy Creek locations underlain by the same geology, but with divergent drying behaviors and distinct stream bed sediments. Specifically, node M759 dried early in 2019 and had large cobbles exposed at the surface, potentially facilitating loss of surface flow to the bed. In contrast, the stream bed at node M1254, approximately 0.5 km further upstream, was characterized by sand and gravel, and surface water persisted year-round. Our observations of fine-scale changes in stream flow presence and coincident changes in streambed materials suggest that shallow subsurface hydraulic conductivity may be a primary spatial control on stream intermittency in Murphy Creek. Stream bed hydraulic conductivity can be highly spatially heterogeneous in space (Schmidt *et al*., 2006, Naganna *et al.,* 2017) and time (Korus *et al.,* 2018, 2020). Given the important role that subsurface properties exert on surface flow variability here and elsewhere (Noorduijn *et al.,* 2014; Quichimbo *et al.,* 2020), metrics such as communication distance can help elucidate spatiotemporal changes in stream network extent. These constraints are critical to understanding connectivity within hydrologic networks and linking to downstream outcomes such as water quantity and quality.

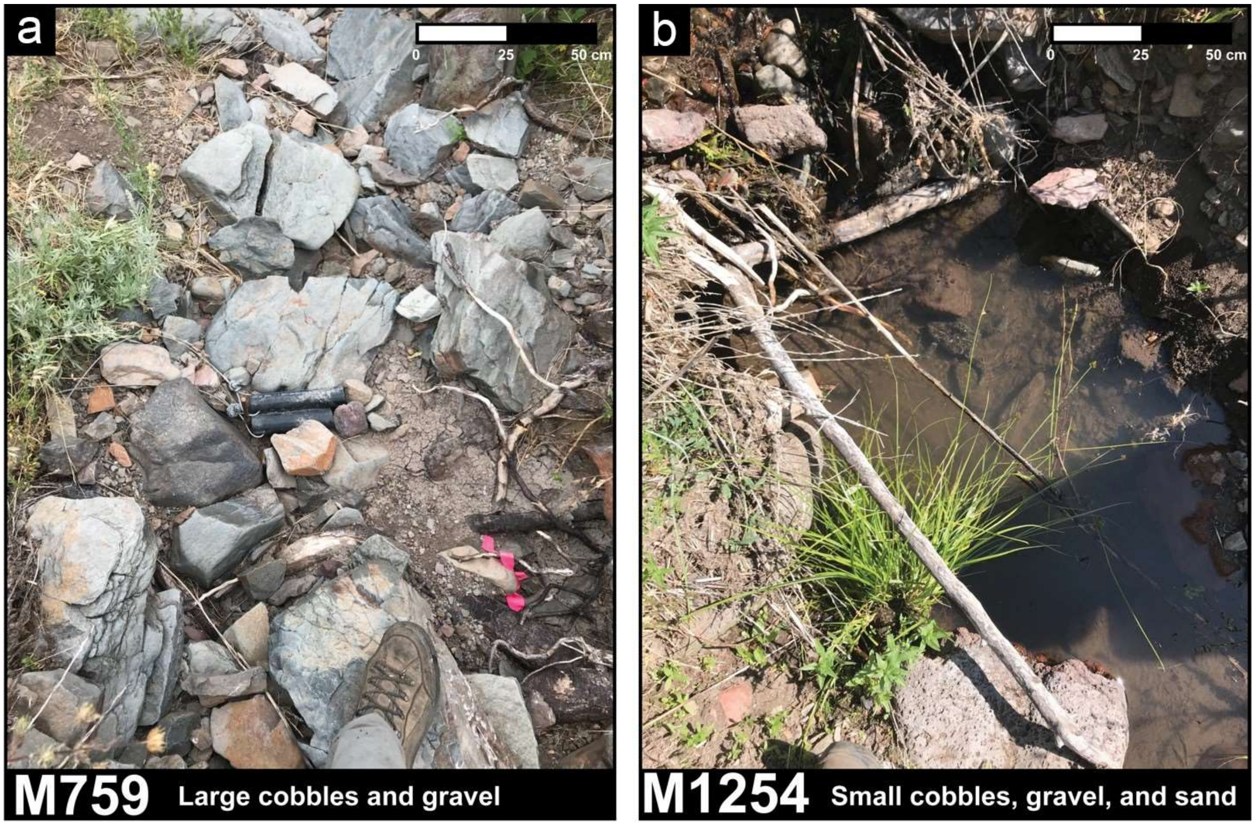

Figure 7. Photos of two sampling locations, (a) M759 and (b) M1254 with different stream subsurface materials, and thus different shallow subsurface porosity, permeability, and hydraulic conductivity (photos: S. Warix).

5.2 Inverse-beta distribution and communication distance identify bottleneck locations at segments that are rarely wet

While mathematical inverses of each other, the beta and inverse-beta distributions did not provide redundant information in our application, allowing additional insights into intermittent stream mechanics. For example, arcs at Murphy Creek that were consistently dry, e.g., $\overrightarrow{INS\ M1993},$ tended have platykurtic inverse-beta posterior distributions for the reciprocal probability of surface water presnece, with particularly large variances (Fig 5). On the other hand, beta posteriors of dry and wet arcs (for the *non-reciprocal* probability of surface water presence) had relatively small variances due to surface water presence outcomes usually being zero or one, respectively (Fig 4).

We used inverse-beta PDFs to represent distributions of reciprocal probabilities of surface water presence. Thus, these distributions depicted patterns in the rarity of arc surface water presence compared to a perennial stream. Communication distance is useful because it leverages the mean value of an arc's inverse-beta posterior as a multiplier for wetted stream length at that arc, and thus defines the average increased effective stream length for communication, compared to a perennial arc. For instance, in the Murphy Creek network, the driest arc, $\overrightarrow{INS\ M1993},$ had a posterior inverse-beta mean of 11.6 (Fig 5b). This indicates that surface water presence at the arc would be, on average, 11.6 times rarer than a perennial arc, and that compared to a perennial stream of the same length, the effective stream length for communication of materials would 11.6 times longer. A posterior inverse-beta mean near one indicates that, on average, an arc behaves essentially identical to a perennial arc for communicating and transporting materials.

5.3 Distinct seasonal variation in active network length, L, and communication distance, C

Although we observed a general trend of increasing resistance to surface transport of materials from spring to summer to fall, the seasonal distributions of communication distance revealed important seasonal differences. Strong negative skew in the fall distributions of $E(C)$ indicated the possibility for good communication periods in this season when water was present, although median communication was poor. The multimodal but smaller-distance distribution of $E(C)$ in the spring occurred because of the strong surface flow persistence of all arcs during early spring, resulting in smaller communication distances, and the late spring drying of several arcs, particularly $\overrightarrow{INS\ M1993}$, resulting in larger communication distances.

Non-redundancy in measures of network communication distance and network Bernoulli stream length were clearly evident in seasonal summaries from Fig 6. Average network Bernoulli stream lengths were longer in the fall compared to summer, indicating a fall rewet period (Fig 6b). This outcome is consistent with regional observations of increased fall discharge (McNamara *et al*. 2005). Evidence of a fall rewet period, however, was not apparent in the posterior distributions of average network communication distance. Instead, larger communication distances were more probable in the fall compared to summer. This discrepancy was due to a marked bifurcation in the behavior of stream arcs in the fall. Specifically, arcs near the outlet and wet spots near the stream center (e.g., $\overrightarrow{M716\ M624}$) tended to be strongly persistent ($\hat{p} \approx 1$), driving larger network stream lengths and smaller communication distances. On the other hand, arcs further from the outlet were often fully absent ($\hat{p} \approx 0$), creating bottlenecks. This outcome was in contrast to the summer, in which posterior variances for $E(C)$ suggested that weak and strong communication outcomes had subequal likelihoods for most segments, and the spring where strong persistency drove smaller distances at all arcs.

Posterior mean Bernoulli stream lengths across all seasons did not approach the full wetted length of Murphy Creek (Fig 6a) due to the moderating effect of conservative prior probabilities from the USGS-PROSPER model (Fig 3a). The PROSPER model is intended to represent the annual probability of stream segment presence, which in the seasonally dry U.S. intermountain west is much lower in the summer than in the fall or spring (Wang et al. 2009). To address the potential detrimental effect of priors on predictive accuracy for a given period, one could decrease the weight of priors in analyses relative to the observed (current) data, or use different priors altogether (although see § 5.4).

5.4 Analytical considerations regarding priors

The USGS-PROSPER model used to define beta prior hyperparameters was suboptimal for our applications. The model incorporates a comprehensive suite of predictors for flow persistence including land use, land cover, soil permeability, topographic wetness index, average maximum and minimum daily temperature, and annual precipitation (Jaeger et al 2019). PROSPER model predictions, however, are not seasonally adjusted and are intended for regional applications rather than fine-scale predictions. We justify our use of these data to define priors due to: 1) the lack of a better alternative, and 2) our view of the PROSPER predictions as provisional long-term representations of the *relative* probability of surface water presence in stream segments at Murphy Creek. Indeed, our work provides an updated prior framework for future Bayesian models.

Our choice of prior weights (w = 0.5) was largely driven by parameter constraints of the inverse-beta posteriors used to calculate mean seasonal communication distances. In particular, infinitely large means for inverse-beta posteriors occurred when zeroes (surface water absences) occurred for all 10 random Bernoulli observations for a segment during drier seasons when the corresponding PROSPER probability of segment surface water presence was 0.21 (the minimum PROSPER probability for the catchment) and the weighting level was $w \leq 0.47$ (Supplemental Materials S2), thus forcing use of weights greater than 0.47. Importantly, larger data sample sizes allow greater flexibility for prior weight choices when faced with outcomes in which no surface flow is observed (see Supplemental Materials S2). Undefined posterior means will not occur for Bayesian extensions of Bernoulli stream length for any $w > 0$. Nonetheless, the same prior weight (w = 0.5) was used for both communication distance and Bernoulli stream length to facilitate comparisons of results under these two approaches.

5.5 Uncertainties and Extensions

Our model predictions concern the probability of surface water presence at stream segments which may not reflect streamflow due to two factors. First, local ponding may lead to surface water without flow. To address this issue, future researchers could combine conductivity and temperature measures *a la* Arismendi *et al*. (2017). These data could then be coupled with appropriate priors to obtain posterior distributions of the probability of stream flow and the reciprocal probability of stream flow at stream arcs. Second, surface networks inferred from very high-resolution topography may be relatively accurate, but those delineated with coarser topographic data that rely on a single area-based threshold (e.g., using the ArcGIS Watershed Toolbox) may require ground-truthing or further consideration, particularly in headwaters, low-gradient systems, or karst regions (Yamazaki *et al.* 2018).

Indeed, although our demonstration considers only surficial stream networks, our field observations suggest that subsurface flow likely dominates Murphy Creek streamflow at certain times of year. In principle, one could model subsurface to surface hydrologic fluxes (e.g., vertical connectivity) and/or subsurface flow using these approaches, by considering the presence/absence of subsurface water with respect todepth or gradient thresholds. In these efforts, the delineation of spatial network structures in the subsurface may be difficult in some locations due to the challenges of defining groundwater arcs and nodes as well as delineating the extent of watersheds (Huggins *et al.,* 2022).

Integration of subsurface connectivity into our methods would allow more holistic considerations of human impacts on the water cycle, as groundwater pumping can cause streams to transitions from perennial to non-perennial flow regimes (Zipper *et al.,* 2022a). Numerous approaches exist to model groundwater pumping impacts on surface streamflow (Zipper *et al.*, 2022b), and analytical models for distributing depletion within stream networks are codified in the **R** package *streamDepletr* (Zipper 2020). Stream vertical connectivity has received relatively little attention (compared to longitudinal surface connectivity) due to the difficulty in obtaining detailed subsurface permeability information (Xiao *et al*. 2021).

Finally, we note that all Bayesian analyses may be strongly affected by prior distribution designations. To address this reality, we recommend the use of sensitivity analyses of putative priors during the formative development of Bayesian models (see Gelman *et al*. 2014, pgs. 160-161, 184-185).

Acknowledgements

This work was made possible with a grant from the National Science Foundation, grant # 2019603, RII Track-2 FEC: Aquatic Intermittency Effects on Microbiomes in Streams (AIMS) and NSF EAR1653998. Thanks to non-author AIMS personnel for their intellectual contributions. The authors declare no real or perceived ethical or financial conflicts of interest.

Open Research

Data for the Murphy Creek network is published (Warix *et al*. 2020) and contained in the **R** package *streamDAG*, maintained by the first author. The package is open source can be downloaded from its repository at https://github.com/moondog1969/streamDAG. Guidance and examples for analyses are provided in the Supplementary Materials and in vignettes within *streamDAG*.

References

Aho, K. A. (2014), *Foundational and Applied Statistics for Biologists using R*. CRC Press.

Aho, K. (2022), *StreamDAG*: Descriptors and methods for stream DAGs. R package version 0.1.2. https://github.com/moondog1969/streamDAG

Aho et al. (2023). Non-perennial stream networks as directed acyclic graphs: The R-package streamDAG. *EarthArXiv*

Ali, G. A., & Roy, A. G. (2009), Revisiting hydrologic sampling strategies for an accurate assessment of hydrologic connectivity in humid temperate systems. *Geography Compass*, *3*(1), 350–374.

Ali, G. A., & Roy, A. G. (2010), Shopping for hydrologically representative connectivity metrics in a humid temperate forested catchment. *Water Resources Research*, *46*(12).

Arismendi, I., Dunham, J. B., Heck, M. P., Schultz, L. D., & Hockman-Wert, D. (2017), A statistical method to predict flow permanence in dryland streams from time series of stream temperature. *Water*, 9 (12), 946.

Barthélemy, J., & Suesse, T. (2018), mipfp: An R package for multidimensional array fitting and simulating multivariate Bernoulli distributions. *Journal of Statistical Software, Code Snippets*, *86*(2), 1–20. https://doi.org/10.18637/jss.v086.c02

Blume, T., & Van Meerveld, H. J. (2015). From hillslope to stream: methods to investigate subsurface connectivity. *Wiley Interdisciplinary Reviews: Water*, *2*(3), 177-198.

Botter, G., & Durighetto, N. (2020), The stream length duration curve: A tool for characterizing the time variability of the flowing stream length. *Water Resources Research*, *56*(8), e2020WR027282.

Bracken, L., Wainwright, J., Ali, G., Tetzlaff, D., Smith, M., Reaney, S., & Roy, A. (2013), Concepts of hydrological connectivity: Research approaches, pathways and future agendas. *Earth-Science Reviews*, *119*, 17–34.

Castellarin, A., Vogel, R. M., & Brath, A. (2004), A stochastic index flow model of flow duration curves. *Water Resources Research*, *40*(3).

Chapin, T. P., Todd, A. S., & Zeigler, M. P. (2014), Robust, low-cost data loggers for stream temperature, flow intermittency, and relative conductivity monitoring. *Water Resources Research*, *50*(8), 6542–6548.

Cressie, N., Frey, J., Harch, B., & Smith, M. (2006), Spatial prediction on a river network. *Journal of Agricultural, Biological, and Environmental Statistics*, *11*(2), 127–150.

Dai, B., Ding, S., & Wahba, G. (2013), Multivariate Bernoulli distribution. *Bernoulli*,19(4), 1465–1483. https://doi.org/10.3150/12-BEJSP10

Dodds, P. S., & Rothman, D. H. (2000). Geometry of river networks. I. Scaling, fluctuations, and deviations. *Physical Review E*, *63*(1), 016115.

Dohman, J. M., Godsey, S. E., & Hale, R. L. (2021). Three-dimensional subsurface flow path controls on flow permanence. *Water Resources Research*, 57, e2020WR028270. https://doi. Org/10.1029/2020WR028270

Dunnington, D. (2021), ggspatial: Spatial data framework for ggplot2. R package version 1.1.5. https://CRAN.R-project.org/package=ggspatial

Fovet, O., Belemtougri, A., Boithias, L., Braud, I., Charlier, J. B., Cottet, M., ... & Datry, T. (2021), Intermittent rivers and ephemeral streams: Perspectives for critical zone science and research on socio-ecosystems. *Wiley Interdisciplinary Reviews: Water*, *8*(4), e1523.

Gelman, A., Carlin, J. B., Stern, H. S., Dunson, D. B., Vehtari, A. & Rubin, D. B. (2014), *Bayesian Data Analysis, 3rd Edition*. Chapman and Hall/CRC.

Godsey S., Kirchner, J. (2014), Dynamic, discontinuous stream networks: hydrologically driven variations in active drainage density, flowing channels and stream order *Hydrological Processes*, 8 (23), 5791-5803.

González-Ferreras, A., & Barquín, J. (2017) Mapping the temporary and perennial character of whole river networks. *Water Resources Research*, 53(8), 6709-6724.

Hale, V. C., & McDonnell, J. J. (2016). Effect of bedrock permeability on stream base flow mean transit time scaling relations: 1. A multiscale catchment intercomparison. *Water Resources Research*, 52(2), 1358-1374.

Hanson, C.L., Marks, D. & Van Vactor, S.S. (2001), Long-term climate database, Reynolds Creek Experimental Watershed, Idaho, USA, *Water Resources Research*, 37, 2839-2841.

Jaeger, K., Sando, R., McShane, R. R., Dunham, J. B., Hockman-Wert, D., Kaiser, K. E., Hafen, K., Risley, J., & Blasch, K. (2019), Probability of streamflow permanence model (PROSPER): A spatially continuous model of annual streamflow permanence throughout the pacific northwest. *Journal of Hydrology X*, *2*, 100005.

Jencso, K. G., McGlynn, B. L., Gooseff, M. N., Wondzell, S. M., Bencala, K. E., & Marshall, L. A. (2009), Hydrologic connectivity between landscapes and streams: Transferring reach-and plot-scale understanding to the catchment scale. *Water Resources Research*, *45*(4).

Kaplan, N. H., Blume, T., & Weiler, M. (2020), Predicting probabilities of streamflow intermittency across a temperate mesoscale catchment. *Hydrology and Earth System Sciences*, *24*(11), 5453-5472.

Knighton, J., Saia, S. M., Morris, C. K., Archiblad, J. A., & Walter, M. T. (2017), Ecohydrologic considerations for modeling of stable water isotopes in a small intermittent watershed. *Hydrological Processes*, *31*(13), 2438-2452.

Korus, J. T., Gilmore, T. E., Waszgis, M. M., & Mittelstet, A. R. (2018). Unit-bar migration and bar-trough deposition: impacts on hydraulic conductivity and grain size heterogeneity in a sandy streambed. *Hydrogeology Journal*, *26*(2), 553-564.

Korus, J. T., Fraundorfer, W. P., Gilmore, T. E., & Karnik, K. (2020). Transient streambed hydraulic conductivity in channel and bar environments, Loup River, Nebraska. *Hydrological Processes*, *34*(14), 3061-3077.

Labbe, T. R., & Fausch, K. D. (2000), Dynamics of intermittent stream habitat regulate persistence of a threatened fish at multiple scales. *Ecological Applications*, *10*(6), 1774-1791.

Larsen, L. G., Choi, J., Nungesser, M. K., & Harvey, J. W. (2012), Directional connectivity in hydrology and ecology. *Ecological Applications*, 22(8), 2204–2220.

Liu, Y., Hou, G., Huang, F., Qin, H., Wang, B., & Yi, L. (2022), Directed graph deep neural network for multi-step daily streamflow forecasting. *Journal of Hydrology*, 607, 127515.

Messager, M. L., Lehner, B., Cockburn, C., Lamouroux, N., Pella, H., Snelder, T., ... & Datry, T. (2021). Global prevalence of non-perennial rivers and streams. *Nature*, *594*(7863), 391-397.

Morita, S., Thall, P. F., & Müller, P. (2008), Determining the effective sample size of a parametric prior. *Biometrics*, *64*(2), 595–602.

Murrell, Z. Wen, Z. (2020), gridGraphics: Redraw base graphics using 'grid' Graphics. R package version 0.5-1. https://CRAN.R-project.org/package=gridGraphics

Naganna, S. R., et al. (2017). Factors influencing streambed hydraulic conductivity and their implications on stream–aquifer interaction: a conceptual review. *Environmental Science and Pollution Research* 24(32): 24765-24789.

Noorduijn, S. L., Shanafield, M., Trigg, M. A., Harrington, G. A., Cook, P. G., & Peeters, L. (2014). Estimating seepage flux from ephemeral stream channels using surface water and groundwater level data. *Water Resources Research*, *50*(2), 1474-1489.

Ort, C., Hollender, J., Schaerer, M., & Siegrist, H. (2009), Model-based evaluation of reduction strategies for micropollutants from wastewater treatment plants in complex river networks. Environmental Science & Technology, 43(9), 3214-3220.

Pebesma, E. (2018), Simple features for R: Standardized support for spatial vector data. The R Journal 10 (1), 439-446. https://doi.org/10.32614/RJ-2018-009

Prancevic, J. P., & Kirchner, J. W. (2019). Topographic controls on the extension and retraction of flowing streams. *Geophysical Research Letters*, *46*(4), 2084-2092.

Quichimbo, E. A., Singer, M. B., & Cuthbert, M. O. (2020). Characterising groundwater–surface water interactions in idealised ephemeral stream systems. *Hydrological Processes*, *34*(18), 3792-3806.

R Core Team. (2022), *R: A language and environment for statistical computing*. R Foundation for Statistical Computing. https://www.R-project.org/

Sando, R., & Blasch, K. W. (2015), Predicting alpine headwater stream intermittency: a case study in the northern Rocky Mountains. *Ecohydrol. Hydrobiol*. 15 (2), 68-80.

Sauquet, E., Shanafield, M., Hammond, J. C., Sefton, C., Leigh, C., & Datry, T. (2021). Classification and trends in intermittent river flow regimes in Australia, northwestern Europe and USA: A global perspective. *Journal of Hydrology*, *597*, 126170.

Schmidt, C., Bayer-Raich, M. & Schirmer, M (2006), Characterization of spatial heterogeneity of groundwater-stream water interactions using multiple depth streambed temperature measurements at the reach scale. *Hydrology and Earth System Sciences* 10(6): 849-859.

Serrano, D., Huggins, X., Gleeson, T., Zipper, S., Jehn, F., Rohde, M. M., Abell, R., Vigerstol, K. & Hartmann, A. (2022). Groundwatersheds of protected areas reveal globally overlooked risks and opportunities. *EarthArXiv*. doi: https://doi.org/10.31223/X59354

Shanafield, M., Bourke, S. A., Zimmer, M. A., & Costigan, K. H. (2021). An overview of the hydrology of non-perennial rivers and streams. *Wiley Interdisciplinary Reviews: Water*, *8*(2), e1504.

Trigg, M. A., Michaelides, K., Neal, J. C., & Bates, P. D. (2013), Surface water connectivity dynamics of a large-scale extreme flood. *Journal of Hydrology*, *505*, 138–149.

USGS. (2016), *StreamStats*. http://streamstats.usgs.gov.

Ver Hoef, J. M., Peterson, E., & Theobald, D. (2006), Spatial statistical models that use flow and stream distance. *Environmental and Ecological Statistics*, *13*(4), 449–464.

Wang, S. Y., Gillies, R. R., Takle, E. S., & Gutowski Jr, W. J. (2009). Evaluation of precipitation in the Intermountain Region as simulated by the NARCCAP regional climate models. *Geophysical Research Letters*, *36*(11).

Warix, S. R., Godsey, S. E., Lohse, K. A., & Hale, R. L. (2021), Influence of groundwater and topography on stream drying in semi-arid headwater streams. *Hydrological Processes*, *35*(5), e14185.

Wickham. 2016. ggplot2: *Elegant Graphics for Data Analysis*. Springer-Verlag New York.

Wilke, C. O. (2020), cowplot: Streamlined plot theme and plot annotations for 'ggplot2'. R package version 1.1.1. https://CRAN.R-project.org/package=cowplot

Xiao, D., Brantley, S. L., & Li, L. (2021). Vertical connectivity regulates water transit time and chemical weathering at the hillslope scale. *Water Resources Research*, 57(8), e2020WR029207.

Yamazaki, D., Ikeshima, D., Sosa, J., Bates, P. D., Allen, G. H., & Pavelsky, T. M. (2019). MERIT Hydro: A high-resolution global hydrography map based on latest topography dataset. *Water Resources Research*, *55*(6), 5053-5073.

Zipper, S. (2020). *streamDepletr*: Estimate streamflow depletion due to groundwater pumping. R package version 0.1.1

Zipper, S. C., Hammond, J. C., Shanafield, M., Zimmer, M., Datry, T., Jones, C. N., et al. & Allen, D. C. (2021). Pervasive changes in stream intermittency across the United States. *Environmental Research Letters*, *16*(8), 084033.

Zipper, S., Popescu, I., Compare, K., Zhang, C., & Seybold, E. C. (2022a). Alternative stable states and hydrological regime shifts in a large intermittent river. *Environmental Research Letters*, *17*(7), 074005.

Zipper, S. C., Farmer, W. H., Brookfield, A., Ajami, H., Reeves, H. W., Wardropper, C., Hammond, J. C., Gleeson, T. & Deines J. M. (2022b). Quantifying Streamflow Depletion from Groundwater Pumping: A Practical Review of Past and Emerging Approaches for Water Management. *Journal of the American Water Resources Association 58*(2), 289–312.